Research Square

Preprints are preliminary reports that have not undergone peer review.
They should not be considered conclusive, used to inform clinical practice,
or referenced by the media as validated information.

Second-law analysis of shell-and-tube and double-pipe heat exchangers operating with Al 2 O 3 /water and TiO 2 /water nanofluids: entropy generation and exergy efficiency from experimental data

Muhammed Elmnefı

muhammed.elmnefi@ostimteknik.edu.tr

Research Article

Keywords: Nanofluid, Exergy analysis, Entropy generation, Shell-and-tube heat exchanger, Double-pipe heat exchanger, Second-law efficiency

Posted Date: November 18th, 2026

DOI: https://doi.org/10.21203/rs.3.rs-11277907/v1

License: This work is licensed under a Creative Commons Attribution 4.0 International License.
Read Full License

Additional Declarations: No competing interests reported.

Second-law analysis of shell-and-tube and double-pipe heat exchangers operating with Al_2O_3/water and TiO_2/water nanofluids: entropy generation and exergy efficiency from experimental data

Muhammed Elmnefi

Department of Aerospace Engineering, Faculty of Engineering, OSTİM Technical University, 06374 Ankara, Türkiye

Corresponding author e-mail: muhammed.elmnefi@ostimteknik.edu.tr; ORCID: 0000-0001-5956-0537

Abstract

Experimental studies of nanofluids in heat exchangers usually report only first-law quantities. This study applies a second-law analysis to previously published measurements from a single test facility containing two counterflow exchangers, one of shell-and-tube type and one of double-pipe type, both run with deionized water and with Al_2O_3/water and TiO_2/water nanofluids at 0.1, 0.2 and 0.3 vol.%. The hot stream was supplied at 60 °C and 7 L/min, while the cold stream was supplied at 30 °C and 5–7 L/min (shell-and-tube) or 2.5–4.5 L/min (double-pipe). Outlet temperatures were reconstructed from the measured heat duties and verified against the reported overall heat transfer coefficients. From these states, the effectiveness, number of transfer units, thermal and frictional entropy generation rates, Bejan number, rate of exergy destruction and second-law efficiency were calculated. In the shell-and-tube exchanger, 0.3 vol.% Al_2O_3/water raised the second-law efficiency by 8.4–11.1% and the exergy delivered to the cold stream by 41.6–63.6% relative to water. In the double-pipe exchanger, the corresponding gains were 7.8–9.1% and 37.3–43.2%. Total entropy generation rose with heat duty, but entropy generated per kilowatt transferred fell by up to 4.4%, so the nanofluids transferred more heat with less irreversibility per unit of heat. The Bejan number exceeded 0.999 in all cases, and the estimated pumping penalty was below 1%. Al_2O_3/water outperformed TiO_2/water at every concentration. The larger benefit in the shell-and-tube exchanger is linked to its low-turbulent tube flow, compared with fully turbulent flow in the double-pipe exchanger.

Keywords: Nanofluid · Exergy analysis · Entropy generation · Shell-and-tube heat exchanger · Double-pipe heat exchanger · Second-law efficiency

List of symbols

Symbol	Meaning (unit)
A	Heat transfer area (m^2)
Be	Bejan number (–)
C	Heat capacity rate, $\dot{m}c_p$ ($W\ K^{-1}$)
c_p	Specific heat ($J\ kg^{-1}\ K^{-1}$)
d_i	Tube inner diameter (m)
f	Darcy friction factor (–)
$\dot{m}$	Mass flow rate ($kg\ s^{-1}$)
NTU	Number of transfer units (–)
Q	Heat transfer rate (W)
$\dot{S}_{gen}$	Entropy generation rate ($W\ K^{-1}$)
T, T_0	Temperature, dead-state temperature (K)
U	Overall heat transfer coefficient ($W\ m^{-2}\ K^{-1}$)
X_d	Exergy destruction rate (W)
ΔP, ΔT_{lm}	Pressure drop (Pa), log-mean temperature difference (K)
ε, η_{II}	Effectiveness, second-law efficiency (–)
ρ, μ, φ	Density ($kg\ m^{-3}$), viscosity (Pa s), volume fraction (–)
Subscripts c, h, i, o	Cold, hot, inlet, outlet
Subscripts bf, np, nf	Base fluid, nanoparticle, nanofluid

1 Introduction

Heat exchangers are central to power generation, process industries, and heating and cooling systems, and improving their performance directly reduces energy use [1, 2]. One of the most widely studied passive enhancement methods is to replace the usual working fluid with a nanofluid, in which nanoparticles are dispersed stably in a carrier liquid [3, 4]. Al_2O_3 and TiO_2 nanoparticles are widely used because they are available, inexpensive and chemically stable in water.

The experimental literature on nanofluid heat exchangers reports mainly first-law quantities: heat transfer rate, convective and overall heat transfer coefficients, and Nusselt number. The author's earlier work took the same approach for two exchangers installed on one rig, of shell-and-tube [5] and double-pipe [6] design, with heat transfer rate increases of up to 49.6% and 32.3%, respectively, for 0.3% Al_2O_3/water. A higher heat transfer rate, however, does not show whether energy is used more efficiently. The second law answers this through entropy generation and exergy destruction, which measure how much work potential is lost in the exchanger [7–9].

Entropy generation in nanofluid flows has been studied extensively, but mostly with numerical models of idealized geometries [10–12]. Experimental second-law studies of nanofluid heat exchangers are fewer, and they usually examine a single tube or one exchanger type [13–18]. Because exchanger geometry, flow range and nanofluid type all affect irreversibility, comparing two exchanger types under the same nanofluids, concentrations and inlet conditions isolates the effect of the exchanger itself. Leong et al. [19] examined theoretically how baffle design changes entropy generation in three shell-and-tube configurations, but, to the author's knowledge, an experimental comparison of two exchanger types on one rig with Al_2O_3/water and TiO_2/water at low concentrations has not been reported.

Table 1 summarizes second-law studies of nanofluid heat exchangers. Most examine a single tube or one exchanger type, often with hybrid or carbon-based nanofluids, and they define exergy efficiency in different ways, so absolute efficiency values are not directly comparable between studies.

Table 1 Previous second-law investigations of nanofluid heat exchangers

Ref.	Heat exchanger	Nanofluid and concentration	Method and flow	Main second-law finding
Leong et al. (2012) [19]	Shell-and-tube; segmental baffles and helical baffles at 25° and 50°	Cu/water, up to 2 vol.%	Theoretical	50° helical baffles gave the least entropy generation; 25° helical baffles gave the most heat transfer
Bahiraei and Mazaheri (2021) [12]	Counter-flow spiral heat exchanger	Al_2O_3/water	Numerical, two-phase mixture model	Second-law analysis aimed at identifying conditions of minimum exergy destruction
Dagdevir and Ozceyhan (2022) [14]	Tube fitted with rod-inserted straight or twisted tape	CuO/water, up to 2.0 mass%	Experimental, turbulent, constant heat flux	Nanofluid raised second-law efficiency; best value 0.44 at Re 6572
Irshad et al. (2022) [15]	Tube heat exchanger	MWCNT–CuO/Therminol 55, 0.005–0.08 mass%	Experimental, turbulent	Exergy efficiency 47.84% against 40.96% for the base fluid at Re 12,500; pumping power up to 103.88% higher
Marulasiddeshi et al. (2023) [16]	Circular copper tube, constant heat flux	Al_2O_3 and Al_2O_3–CuO/water, inlet 30–60 °C	Experimental	Entropy generation and exergy analysed over a range of Reynolds numbers; the hybrid nanofluid outperformed Al_2O_3 alone
Mertaslan and Keklikcioglu (2024) [17]	Tube with coiled-wire inserts	GnP–Fe_3O_4/water–ethylene glycol, 0.2–0.4 mass%	Experimental, Re 3000–15,000, constant heat flux	Highest second-law efficiency 0.416; Bejan number 0.93–0.98, heat transfer irreversibility dominant
Azharuddin and Saini (2025) [18]	Shell-and-tube	$AgNO_3$–graphene/water, 0.01–0.03 vol.%	Experimental, 115–155 L/h	At 0.03 vol.%, exergy efficiency rose by 70.01% (shell side) and 32.72% (tube side)
Present study	Two exchanger types (shell-and-tube, double-pipe)	Al_2O_3/water and TiO_2/water, 0.1–0.3 vol.%	Experimental data, Re 3050–10,000	Second-law efficiency up 8.4–11.1% (shell-and-tube) and 7.8–9.1% (double-pipe) for 0.3% Al_2O_3; Bejan number above

Ref.	Heat exchanger	Nanofluid and concentration	Method and flow	Main second-law finding
	on one rig			0.999

This study therefore performs a second-law analysis of the experimental data from both exchangers. Its objectives are to: (i) reconstruct the full thermal state of every operating point from the published measurements and check its consistency; (ii) evaluate the first- and second-law performance indicators of water and of both nanofluids; (iii) compare the two exchanger types; and (iv) assess how measurement uncertainty affects the conclusions.

2 Experimental data and reconstruction of operating states

2.1 Test rig and data sources

Fig. 1 summarizes the analysis procedure. Both exchangers were installed on one rig with a common hot loop and cold loop [5, 6]. In every test the hot water was supplied at 60 °C and 7 L/min, and the cold fluid was supplied at 30 °C in counterflow. The nanofluids were prepared from Al_2O_3 (28 nm) and TiO_2 (25–45 nm) nanopowders of 99.99% purity at 0.1, 0.2 and 0.3 vol.%. Table 2 summarizes the two exchangers and the source of each data set.

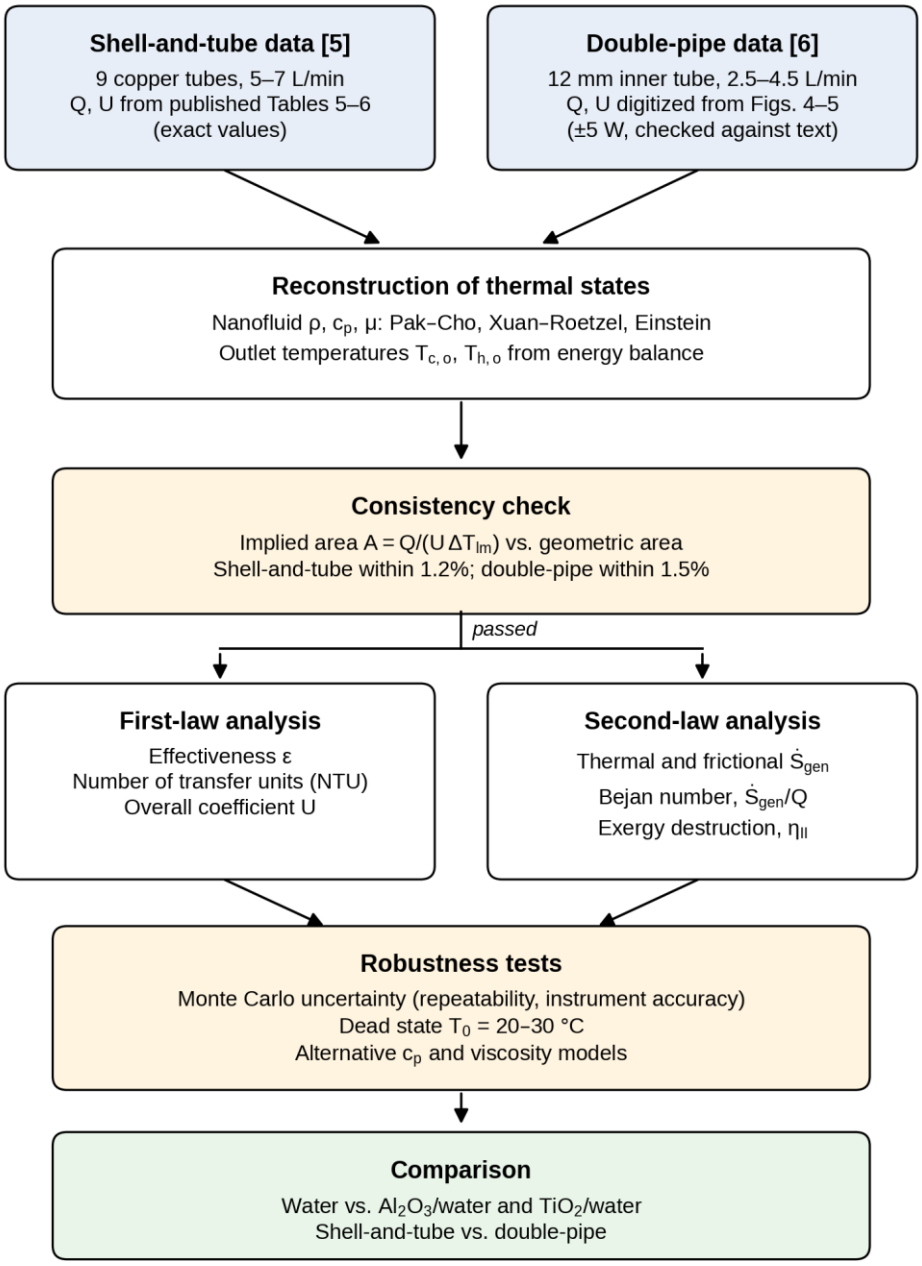


Fig. 1 *Methodology of the second-law analysis based on published experimental data*

Table 2 Main features of the two heat exchangers and sources of the data

Item	Shell-and-tube	Double-pipe
Cold fluid side	9 copper tubes, d_i = 4.826 mm, L = 370 mm	Copper inner tube, d_i = 12 mm, L = 1000 mm
Hot fluid side	Galvanized iron shell, D_i = 57 mm	Iron outer pipe, D_i = 36 mm
Cold flow rates (L/min)	5, 5.5, 6, 6.5, 7	2.5, 3, 3.5, 4, 4.5
Source of Q and U	Tables 5 and 6 of Ref. [5]	Figs. 4 and 5 of Ref. [6], digitized (Appendix A)
Operating points	35	35

For the shell-and-tube unit, Q and U were read directly from the tables of Ref. [5]. For the double-pipe exchanger, they were extracted from the published figures and checked against

the values stated in the text: 1339 W against the stated 1340 W for Q, and 1696 against 1693.5 W m^{-2} K^{-1} for U, both for 0.3% Al_2O_3 at 4.5 L/min. Water values read from the three panels of Fig. 4 of Ref. [6] differed by at most 6 W, so the reading uncertainty is about ±5 W (±0.5%).

2.2 Reconstruction of outlet temperatures

The original temperature records were not retained, so outlet temperatures were reconstructed from Q, the known inlet temperatures and the flow rates. Assuming negligible heat loss, as in the original studies, the cold and hot outlet temperatures are

$$T_{\mathrm{c,o}} = T_{\mathrm{c,i}} + \frac{Q}{\dot{m}_{\mathrm{c}}\, c_{p,\mathrm{c}}} \tag{1}$$

$$T_{\mathrm{h,o}} = T_{\mathrm{h,i}} - \frac{Q}{\dot{m}_{\mathrm{h}}\, c_{p,\mathrm{h}}} \tag{2}$$

The reconstruction (Eqs. 1 and 2) was checked by recomputing the heat transfer area implied by the published U and the reconstructed log-mean temperature difference, $A = Q/(U\,\Delta T_{lm})$. For the shell-and-tube unit, this back-calculated area was 0.0499 ± 0.0003 m^2 across all 35 points, within 1.2% of the geometric inner tube area of 0.0505 m^2. This confirms that the reconstructed temperatures are consistent with the published data. For the double-pipe exchanger, using the digitized U of water and 0.3% Al_2O_3, the implied area was 0.0297–0.0301 m^2, within 1.5% of the inner-tube area over the 0.8 m heat transfer length (0.0302 m^2).

3 Thermodynamic analysis

3.1 Nanofluid properties

As in the original studies, the density and specific heat of each nanofluid followed the mixing rules of Pak and Cho [20] and Xuan and Roetzel [21], and its viscosity followed the Einstein relation:

$$\rho_{\mathrm{nf}} = (1-\phi)\,\rho_{\mathrm{bf}} + \phi\,\rho_{\mathrm{np}} \tag{3}$$

$$c_{p,\mathrm{nf}} = \frac{(1-\phi)\,\rho_{\mathrm{bf}}\, c_{p,\mathrm{bf}} + \phi\,\rho_{\mathrm{np}}\, c_{p,\mathrm{np}}}{\rho_{\mathrm{nf}}} \tag{4}$$

$$\mu_{\mathrm{nf}} = \mu_{\mathrm{bf}}\,(1 + 2.5\,\phi) \tag{5}$$

Base-fluid properties were taken as ρ = 996 kg m^{-3}, c_p = 4178 J kg^{-1} K^{-1} and μ = 7.97 × 10^{-4} Pa s, and hot water as ρ = 983.2 kg m^{-3} and c_p = 4184 J kg^{-1} K^{-1}. Particle properties were ρ =

102 3900 kg m^{-3} and c_p = 895 J kg^{-1} K^{-1} for Al_2O_3, and ρ = 4500 kg m^{-3} and c_p = 689.36 J kg^{-1} K^{-1}
103 for TiO_2.

104 **3.2 Effectiveness and NTU**

105 With C_{min} the smaller heat capacity rate, effectiveness and NTU (Eqs. 6 and 7) follow from
106 the heat duty and log-mean temperature difference. Writing NTU this way makes it
107 independent of the area definition:

$$\varepsilon = \frac{Q}{C_{\min}\left(T_{\mathrm{h,i}} - T_{\mathrm{c,i}}\right)} \tag{6}$$

$$\mathrm{NTU} = \frac{UA}{C_{\min}} = \frac{Q}{C_{\min}\,\Delta T_{\mathrm{lm}}} \tag{7}$$

108 **3.3 Entropy generation**

109 Treating both streams as incompressible, the entropy produced because heat crosses a finite
110 temperature difference is [7]

$$\dot{S}_{\mathrm{gen},\Delta T} = \dot{m}_{\mathrm{c}}\, c_{p,\mathrm{c}} \ln\frac{T_{\mathrm{c,o}}}{T_{\mathrm{c,i}}} + \dot{m}_{\mathrm{h}}\, c_{p,\mathrm{h}} \ln\frac{T_{\mathrm{h,o}}}{T_{\mathrm{h,i}}} \tag{8}$$

111 This split into thermal and frictional parts follows earlier entropy analyses of nanofluid flow
112 in tubes [22, 23]. Pressure drop was not measured, so the tube-side pressure drop of the
113 nanofluid was estimated from the Blasius friction factor and the Darcy–Weisbach relation:

$$f = 0.316\,\mathrm{Re}^{-0.25} \tag{9}$$

$$\Delta P = f\,\frac{L}{d_{\mathrm{i}}}\,\frac{\rho V^2}{2} \tag{10}$$

114 The frictional entropy generation and the Bejan number then follow as

$$\dot{S}_{\mathrm{gen},\Delta P} = \frac{\dot{m}_{\mathrm{c}}\,\Delta P}{\rho_{\mathrm{c}}\,T_{\mathrm{c,m}}} \tag{11}$$

$$\mathrm{Be} = \frac{\dot{S}_{\mathrm{gen},\Delta T}}{\dot{S}_{\mathrm{gen},\Delta T} + \dot{S}_{\mathrm{gen},\Delta P}} \tag{12}$$

115 Tube lengths of 0.37 m (shell-and-tube) and 1.0 m (double-pipe) were used. Hot-side friction
116 was excluded because the hot-side flow was identical in every test and its contribution does
117 not change between fluids. To compare fluids that transfer different amounts of heat, entropy
118 generation is also reported per unit heat duty, $\dot{S}_{gen}/Q$ (W K^{-1} per kW).

3.4 Exergy destruction and efficiency

With a dead state of T_0 = 298.15 K (its effect is examined in Section 5.4), exergy destruction follows from the total entropy generation through the Gouy–Stodola relation:

$$\dot{X}_{\mathrm{d}} = T_0 \left(\dot{S}_{\mathrm{gen},\Delta T} + \dot{S}_{\mathrm{gen},\Delta P} \right) \tag{13}$$

The second-law efficiency is defined as the ratio of the exergy increase of the cold fluid to the exergy decrease of the hot fluid:

$$\eta_{\mathrm{II}} = \frac{\dot{m}_{\mathrm{c}}\, c_{p,\mathrm{c}} \left[\left(T_{\mathrm{c,o}} - T_{\mathrm{c,i}} \right) - T_0 \ln \frac{T_{\mathrm{c,o}}}{T_{\mathrm{c,i}}} \right]}{\dot{m}_{\mathrm{h}}\, c_{p,\mathrm{h}} \left[\left(T_{\mathrm{h,i}} - T_{\mathrm{h,o}} \right) - T_0 \ln \frac{T_{\mathrm{h,i}}}{T_{\mathrm{h,o}}} \right]} \tag{14}$$

4 Uncertainty analysis

The absolute values of Q and $\dot{S}_{\mathrm{gen}}$ carry large instrument uncertainty, but the second-law efficiency and the comparisons between fluids are robust. Uncertainty was propagated by Monte Carlo simulation (2×10^5 samples) at 7 L/min for two scenarios. The first uses the repeatability reported in the original studies (standard error 0.0334 K per temperature). The second uses the manufacturer accuracy of the K-type thermocouples (±1 °C) and flowmeters (±5%), treated as uniform distributions. Table 3 gives the results.

Table 3 Relative standard uncertainty of the main results for the shell-and-tube exchanger at 7 L/min

Quantity	Repeatability, water	Repeatability, 0.3% Al_2O_3	Instrument accuracy, water	Instrument accuracy, 0.3% Al_2O_3
Q	2.0%	1.3%	34.1%	22.9%
$\dot{S}_{\mathrm{gen}}$	1.8%	1.1%	31.5%	20.0%
η_{II}	0.4%	0.4%	7.5%	7.0%

The instrument scenario is dominated by the small cold-side temperature rise (2.4–4.1 K) relative to the ±1 °C thermocouple accuracy. Two points limit its effect on the conclusions. First, η_{II} depends on the ratio of cold-side to hot-side exergy change, so its uncertainty is several times smaller than that of Q. Second, every fluid was measured with the same thermocouples, and a fixed calibration offset shifts all fluids in the same direction; it therefore affects absolute values more than the differences between fluids. The trends reported in Section 5 should nevertheless be read as relative comparisons. All thermocouples were calibrated before testing. Calibration removes most of the fixed offset between sensors, so the

instrument-accuracy scenario above is a conservative upper bound, and the actual uncertainty lies between the two scenarios.

5 Results and discussion

5.1 Shell-and-tube heat exchanger

All nanofluids raised effectiveness, NTU and second-law efficiency above water (Fig. 2), and the gain grew with concentration and was larger for Al_2O_3 than for TiO_2. Table 4 gives the results at the highest flow rate, where the differences between fluids are largest.

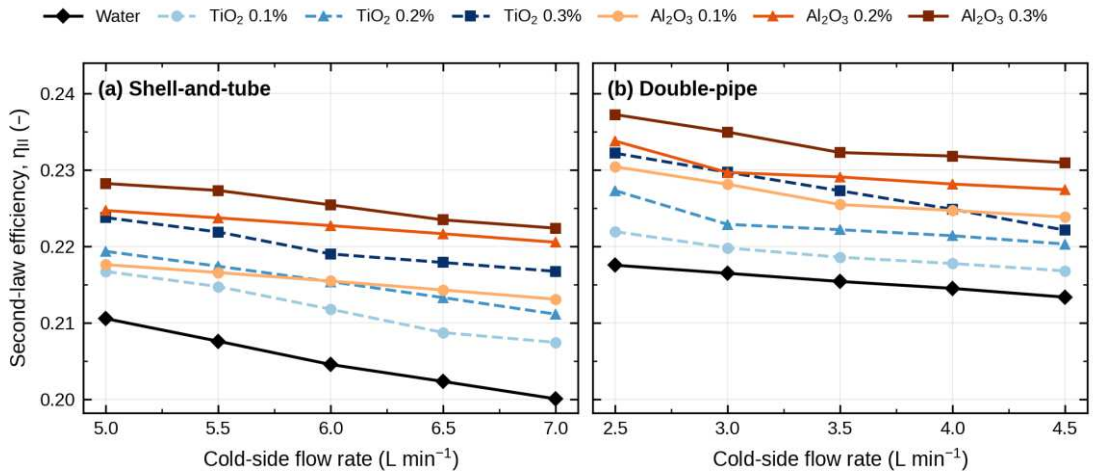


Fig. 2 *Second-law efficiency versus cold flow rate: (a) shell-and-tube and (b) double-pipe heat exchanger*

Table 4 Shell-and-tube unit: first- and second-law results at 7 L/min cold-side flow

Fluid	ε	NTU	$\dot{S}_{gen}$ (W K^{-1})	$\dot{S}_{gen}$/Q (W K^{-1} per kW)	X_d (W)	Exergy gained by cold stream (W)	η_{II}	$\Delta\eta_{II}$ vs. water
Water	0.081	0.088	0.318	0.273	94.9	23.7	0.200	–
TiO_2 0.1%	0.094	0.104	0.366	0.269	109.0	28.5	0.207	+3.7%
TiO_2 0.2%	0.101	0.112	0.388	0.267	115.8	31.0	0.211	+5.5%
TiO_2 0.3%	0.111	0.125	0.422	0.264	125.8	34.8	0.217	+8.3%
Al_2O_3 0.1%	0.104	0.117	0.400	0.266	119.4	32.3	0.213	+6.5%
Al_2O_3 0.2%	0.118	0.133	0.445	0.262	132.6	37.5	0.221	+10.2%
Al_2O_3 0.3%	0.121	0.138	0.455	0.261	135.7	38.8	0.222	+11.1%

Effectiveness and NTU. Effectiveness was low for all fluids (0.08–0.14) because the exchanger is short and both streams have similar heat capacity rates. It fell as cold flow rate

rose: for water, from 0.103 at 5 L/min to 0.081 at 7 L/min. The 0.3% Al_2O_3 nanofluid raised effectiveness by 32–50% across the flow range.

Entropy generation. Total entropy generation rose with heat duty, from 0.290–0.318 W K^{-1} for water to 0.371–0.455 W K^{-1} for 0.3% Al_2O_3. This rise is expected: a fluid that transfers more heat across the same 26–27 K stream temperature difference generates more entropy. The fair comparison is entropy generated per kilowatt transferred (Fig. 3). It fell from 0.270–0.273 W K^{-1} per kW for water to 0.261–0.262 W K^{-1} per kW for 0.3% Al_2O_3, a reduction of 3.2–4.4%. This agrees with the analytical second-law study of Moghaddami et al. [24], which showed that adding Al_2O_3 nanoparticles can reduce entropy generation in tube flow and identified optimum operating conditions for both laminar and turbulent regimes. The nanofluids therefore transferred heat more reversibly, because the larger cold-side temperature rise reduced the mean temperature difference between the streams.

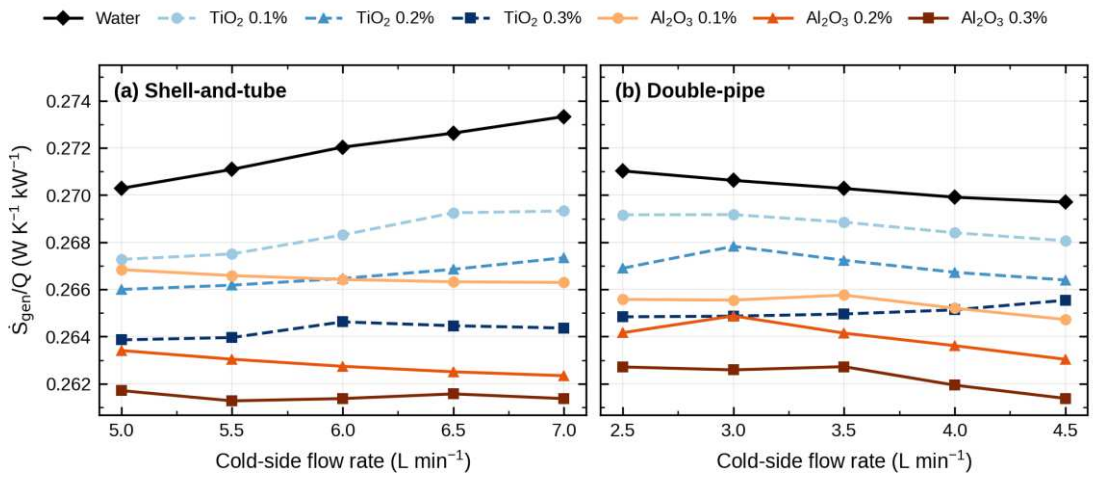


Fig. 3 *Entropy generated per kilowatt transferred versus cold flow rate: (a) shell-and-tube and (b) double-pipe heat exchanger*

Bejan number and friction. The Bejan number exceeded 0.999 for every case. The estimated tube-side frictional entropy generation was only 0.11–0.29 mW K^{-1}, against 290–455 mW K^{-1} from heat transfer. The Einstein viscosity increase at 0.3% raised the estimated pumping power by less than 1% (from 87.4 to 88.2 mW at 7 L/min). At these low concentrations, the frictional penalty of the nanofluids is negligible on a second-law basis. This agrees with experimental tube studies in which heat-transfer irreversibility dominated and the Bejan number stayed close to unity [17]. At higher particle loadings friction can matter: for TiO_2/MWCNT hybrid nanofluids in pipe flow, exergy efficiency peaked at 0.1 vol.%, not at the largest loading tested (0.3 vol.%), because frictional losses grew with

loading [25]. Likewise, turbulent tube experiments with a fly ash–Cu hybrid suspension showed lower entropy generation at higher particle loading [26]. Within the estimated friction of the present low-concentration oxide nanofluids, no such trade-off appears.

Exergy and second-law efficiency. The exergy delivered to the cold stream (Fig. 4) rose by 14.1–20.2% for 0.1% TiO_2 and by 41.6–63.6% for 0.3% Al_2O_3. Second-law efficiency rose by 2.9–8.3% for TiO_2 and 3.4–11.1% for Al_2O_3, with the largest gains at the highest flow rate. Larger improvements, based on a different efficiency definition, were reported for a hybrid nanofluid in a shell-and-tube unit [18], and improvements in exergy efficiency were also measured with nanodiamond suspensions in a coiled-tube exchanger [27]. With every fluid, η_{II} decreased slightly as flow rate increased (for water from 0.211 to 0.200), because a higher cold flow rate lowers the cold outlet temperature and with it the quality of the delivered heat. Absolute η_{II} values near 0.2 are typical of low-temperature water-to-water exchangers, where the cold stream is heated only a few kelvin above the dead state.

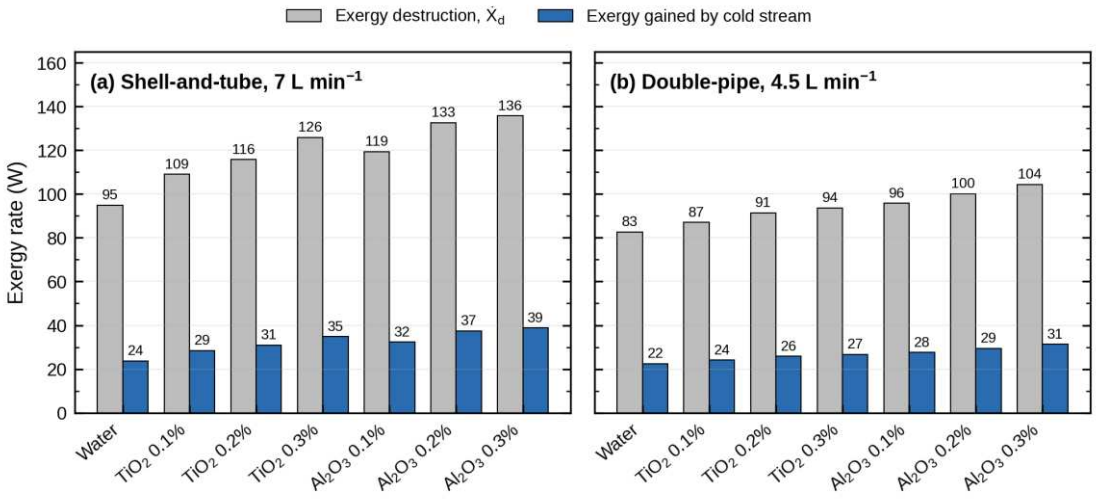


Fig. 4 *Exergy destruction and exergy gained by the cold stream at the highest flow rate: (a) shell-and-tube, 7 L/min and (b) double-pipe, 4.5 L/min*

5.2 Double-pipe heat exchanger

The trends for the double-pipe unit were the same: every nanofluid improved all second-law measures, and Al_2O_3 again outperformed TiO_2 at each concentration. The weaker performance of TiO_2 agrees with a recent review of TiO_2 nanofluids in double-pipe exchangers, which found TiO_2 better than water but weaker than most other common nanofluids [28]. Earlier double-pipe experiments with TiO_2/water [29], with several nanofluids in double-tube exchangers [30], and with a TiO_2 suspension in ethylene glycol–

water flowing through a spiral double-tube unit [31] concentrated mainly on first-law performance, so the present second-law results have few direct counterparts for this exchanger type. Table 5 gives the results at the highest flow rate.

Table 5 Double-pipe unit: first- and second-law results at 4.5 L/min cold-side flow

Fluid	ε	NTU	$\dot{S}_{gen}$ (W K^{-1})	$\dot{S}_{gen}/Q$ (W K^{-1} per kW)	X_d (W)	Exergy gained by cold stream (W)	η_{II}	$\Delta\eta_{II}$ vs. water
Water	0.110	0.121	0.277	0.270	82.7	22.4	0.213	–
TiO_2 0.1%	0.116	0.129	0.292	0.268	87.0	24.1	0.217	+1.6%
TiO_2 0.2%	0.123	0.137	0.307	0.266	91.4	25.8	0.220	+3.3%
TiO_2 0.3%	0.126	0.141	0.314	0.266	93.7	26.7	0.222	+4.1%
Al_2O_3 0.1%	0.130	0.145	0.321	0.265	95.8	27.6	0.224	+4.9%
Al_2O_3 0.2%	0.136	0.154	0.336	0.263	100.1	29.5	0.227	+6.6%
Al_2O_3 0.3%	0.143	0.162	0.350	0.261	104.3	31.3	0.231	+8.2%

Effectiveness and NTU. Effectiveness rose from 0.110–0.124 for water to 0.143–0.163 for 0.3% Al_2O_3, and fell with increasing flow rate as in the shell-and-tube exchanger.

Entropy generation. The total entropy generation increased from 0.174–0.277 W K^{-1} (water) to 0.223–0.350 W K^{-1} for 0.3% Al_2O_3. Entropy generated per kilowatt fell from 0.270–0.271 W K^{-1} per kW for water to 0.261–0.263 W K^{-1} per kW for 0.3% Al_2O_3, a reduction of 2.8–3.1%. For 0.3% TiO_2, the reduction was 1.5–2.3%.

Bejan number and friction. The Bejan number exceeded 0.999. Estimated frictional entropy generation was 0.03–0.14 mW K^{-1} and pumping power 8.6–43.7 mW, with the nanofluids adding less than 1% to either.

Exergy and second-law efficiency. The exergy delivered to the cold stream rose by 6.7–9.2% for 0.1% TiO_2 and by 37.3–43.2% for 0.3% Al_2O_3. Second-law efficiency rose by 1.5–6.7% for TiO_2 and 4.7–9.1% for Al_2O_3. Unlike in the shell-and-tube exchanger, the gain for 0.3% TiO_2 was largest at the lowest flow rate (6.7% at 2.5 L/min, 4.1% at 4.5 L/min), following its first-law enhancement in Fig. 4 of Ref. [6], which falls from 23.8% to 15.1% over the same range.

5.3 Comparison of the two exchangers

The shell-and-tube exchanger benefited more from the nanofluids on every second-law measure, even though the double-pipe exchanger performed better with water alone (Table 6).

Table 6 Side-by-side comparison of the two exchangers

Measure	Shell-and-tube	Double-pipe
Tube-side Reynolds number	3050–4300	5500–10,000
Heat transfer area (m^2)	0.050	0.030
Water: overall coefficient U ($W\ m^{-2}\ K^{-1}$)	797–859	780–1252
Water: cold-side temperature rise (K)	2.4–3.1	3.3–3.7
Water: η_{II}	0.200–0.211	0.213–0.218
Water: $\dot{S}_{gen}/Q$ ($W\ K^{-1}$ per kW)	0.270–0.273	0.270–0.271
0.3% Al_2O_3: gain in Q	31.9–49.6%	28.2–32.0%
0.3% Al_2O_3: gain in η_{II}	8.4–11.1%	7.8–9.1%
0.3% Al_2O_3: reduction in $\dot{S}_{gen}/Q$	3.2–4.4%	2.8–3.1%
0.3% Al_2O_3: gain in cold-stream exergy	41.6–63.6%	37.3–43.2%

Baseline performance. With water, the double-pipe exchanger reached a U up to 46% higher with 40% less area, because flow in its single 12 mm tube was fully turbulent, whereas flow in the nine 4.8 mm tubes of the other unit remained only weakly turbulent. Its lower cold flow rates also gave a larger cold-side temperature rise, which explains its slightly higher η_{II}.

Entropy per unit heat is set by the inlet temperatures. For water, $\dot{S}_{gen}/Q$ was almost identical in both exchangers (0.270–0.273 $W\ K^{-1}$ per kW), although their geometry, area and flow range differ widely. With both streams entering at 60 °C and 30 °C and warming or cooling only a few kelvin, this quantity is fixed mainly by the inlet temperatures. A nanofluid lowers it only by raising the cold outlet temperature, which is why its reduction tracks the first-law gain.

Why the shell-and-tube exchanger gained more. The nanofluid gains followed the first-law enhancements (Fig. 5), which were larger in the shell-and-tube exchanger. The relation is almost linear: each 1% increase in heat transfer rate raised η_{II} by about 0.23% in the shell-and-tube exchanger ($R^2 = 0.980$) and by about 0.28% in the double-pipe exchanger ($R^2 = 0.999$), for both nanoparticle types. Hence the shell-and-tube unit gains more on a second-law basis simply because its first-law enhancement is larger, and not because it converts that enhancement into exergy more effectively. Earlier shell-and-tube experiments with oxide nanofluids also reported clear heat transfer gains [32, 33]. A plausible explanation is the flow regime: in low-turbulent flow, the thermal resistance of the near-wall layer is a larger share of the total, so changes in the fluid near the wall have more effect than in fully turbulent flow. Recent pipe-flow measurements support this: nanofluid Nusselt number enhancement exceeded 29% in transitional flow but reached at most 7.7% in turbulent flow [25]. Experimental second-law data for Al_2O_3–MWCNT hybrid suspensions in transitional flow are

also available [34]. This explanation should be tested with measured thermophysical properties and pressure drop in future work.

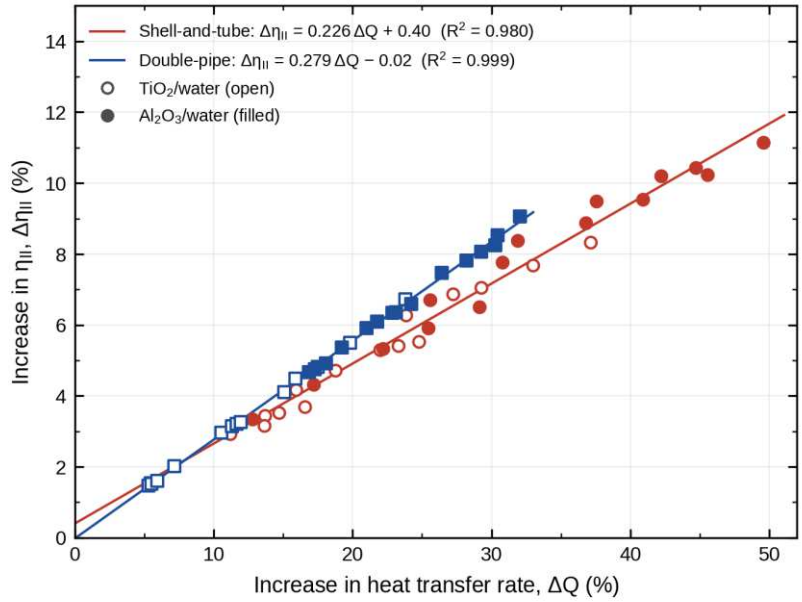


Fig. 5 *Relative increase in second-law efficiency versus relative increase in heat transfer rate for both heat exchangers. Open symbols: TiO_2/water; filled symbols: Al_2O_3/water; lines: least-squares fits*

5.4 Sensitivity to the dead state and property models

The main conclusions do not depend on the choice of dead-state temperature or nanofluid property models, although absolute second-law efficiencies do.

Dead-state temperature. The analysis was repeated with T_0 = 20 and 30 °C (Table 7). Absolute η_{II} changes strongly with T_0 because the cold stream enters at 30 °C, close to the dead state: at T_0 = 30 °C it enters exactly at the dead state, so its exergy gain is small and relative improvements appear large. At all three dead-state temperatures, every nanofluid at every flow rate had a higher η_{II} than water. The gain range was 1.7–6.6% at 20 °C and 11.6–52.2% at 30 °C for the shell-and-tube exchanger, and 0.9–5.3% and 5.4–32.6% for the double-pipe exchanger. Exergy destruction changed by less than 2%, and entropy generation, including $\dot{S}_{gen}/Q$, does not depend on T_0 at all. Relative η_{II} gains should therefore always be reported together with the chosen dead state.

Table 7 Second-law efficiency at the highest flow rate for three dead-state temperatures

T_0 (°C)	Shell-and-tube, water	Shell-and-tube, 0.3% Al_2O_3	Gain	Double-pipe, water	Double-pipe, 0.3% Al_2O_3	Gain
20	0.315	0.336	+6.6%	0.326	0.342	+4.9%
25	0.200	0.222	+11.1%	0.213	0.231	+8.2%

T_0 (°C)	Shell-and-tube, water	Shell-and-tube, 0.3% Al_2O_3	Gain	Double-pipe, water	Double-pipe, 0.3% Al_2O_3	Gain
30	0.045	0.069	+52.2%	0.062	0.081	+31.4%

Property models. Replacing the Xuan and Roetzel specific heat relation [21] with a simple mass-weighted average changed η_{II} by at most 0.23% and $\dot{S}_{gen}/Q$ by at most 0.07%. At these concentrations the Brinkman viscosity model gives the same result as the Einstein relation to within 0.01%. As an upper bound, the empirical viscosity correlation of Pak and Cho [20] for Al_2O_3/water was applied to both nanofluids; it predicts a 12% higher viscosity at 0.3%. Even then, the estimated pumping power rose only 3.6–3.7% above water, frictional entropy generation stayed below 0.30 mW K^{-1}, and the Bejan number remained above 0.999. The conclusion that friction is negligible on a second-law basis therefore holds under a much more conservative viscosity assumption.

5.5 Limitations

Four limitations should be kept in mind when using these results.

1. Pressure drop was not measured, so frictional entropy generation and pumping power were estimated from the Blasius correlation and viscosity models. Because frictional irreversibility was about three orders of magnitude smaller than thermal irreversibility, even a large error in this estimate would not change the conclusions (Section 5.4).
2. Nanofluid properties were calculated from models rather than measured. Only density and specific heat enter the second-law results, and the choice of model changed η_{II} by less than 0.25%.
3. Outlet temperatures were reconstructed by energy balance, and the double-pipe data were digitized from published figures, because the original temperature records were not retained. The area check in Section 2.2 and the agreement with values stated in the original papers support this approach, but the data cannot be checked against raw measurements.
4. The cold-side temperature rise was small compared with the thermocouple accuracy, so absolute values carry larger uncertainty than the comparisons between fluids (Section 4). Heat loss to the surroundings and hot-side friction were also neglected, as in the original studies.

6 Conclusions

Published measurements from two exchangers, of shell-and-tube and double-pipe design, running with water and with 0.1–0.3 vol.% Al_2O_3 and TiO_2 suspensions in water were re-examined on a second-law basis. The main conclusions are:

1. Outlet temperatures reconstructed from the published heat duties were consistent with the published U values: the back-calculated area agreed with the true tube area to within 1.2%.

2. In the shell-and-tube exchanger, the nanofluids raised second-law efficiency by 2.9–11.1% and the exergy delivered to the cold stream by up to 63.6%. The best fluid was 0.3% Al_2O_3/water at 7 L/min.
3. Total entropy generation rose with heat duty, but entropy generated per kilowatt transferred fell by up to 4.4%. The nanofluids transferred more heat with less irreversibility per unit of heat.
4. The Bejan number exceeded 0.999 in all cases, and the estimated pumping power penalty was below 1%. At these concentrations, the frictional cost of the nanofluids is negligible.
5. Al_2O_3/water outperformed TiO_2/water at every concentration and flow rate on both first-law and second-law measures.
6. In the double-pipe exchanger, the nanofluids raised second-law efficiency by 1.5–9.1% and cold-stream exergy by up to 43.2%. The gains were smaller than in the shell-and-tube exchanger, whose tube flow was low-turbulent (Re 3050–4300) rather than fully turbulent (Re 5500–10,000). For water, entropy generated per kilowatt was almost the same in both exchangers (0.270–0.273 W K^{-1} per kW), showing that it is set mainly by the inlet temperatures. All of these conclusions held for dead-state temperatures of 20–30 °C and for alternative specific heat and viscosity models.

Future experimental work should measure pressure drop and nanofluid thermophysical properties directly and use more accurate temperature sensors, such as calibrated RTDs or differential thermocouples, to reduce the uncertainty of the small cold-side temperature rise. The same reconstruction and second-law approach can also be applied to other nanofluid thermal systems, for example the CuO/synthetic oil parabolic trough collector investigated earlier by the author [35].

Appendix A Digitized double-pipe data

Heat transfer rate Q (W) read from Fig. 4 of Ref. [6]; water is the mean of the three panels. Reading uncertainty is about ±5 W.

Table A1 Digitized heat transfer rate Q (W) of the double-pipe exchanger

Flow rate (L/min)	Water	TiO_2 0.1%	TiO_2 0.2%	TiO_2 0.3%	Al_2O_3 0.1%	Al_2O_3 0.2%	Al_2O_3 0.3%
2.5	643	689	745	796	778	813	849
3.0	749	790	828	912	893	912	977
3.5	848	893	944	1016	991	1042	1087
4.0	943	995	1053	1108	1106	1161	1219
4.5	1028	1089	1151	1183	1214	1277	1339

Table A2 Digitized U values (W m^{-2} K^{-1}) of the double-pipe unit, used in the area check

Flow rate (L/min)	Water	Al_2O_3 0.3%
2.5	780	1069
3.0	908	1227
3.5	1031	1375
4.0	1148	1541
4.5	1252	1696

Declarations

Funding No funding was received for conducting this study.

Competing interests The author has no relevant financial or non-financial interests to disclose.

Author contributions M.E., as sole author, was responsible for the study concept, methods, analysis, figures and text.

Data availability The experimental data analysed in this study were published in Refs. [5, 6]. The digitized double-pipe data are given in Appendix A, and the calculated second-law results are available from the author on reasonable request.

Use of AI tools During the preparation of this work, the author used Claude (Anthropic), an AI assistant, to support digitization of published figures, data analysis code, literature searching, preparation of figures, and drafting and language editing of the text. The author verified all data, calculations and references, revised the manuscript, and takes full responsibility for its content.

Acknowledgements The author thanks Raed Abdullah and Mohanad Al-Sammarraie, co-authors of the original experimental studies [5, 6], for their contribution to the measurements analysed here.

References

1. Master BI, Chunangad KS, Boxma AJ, Kral D, Stehlík P. Most frequently used heat exchangers from pioneering research to worldwide applications. Heat Transf Eng. 2006;27(6):4–11.
2. Pordanjani AH, Aghakhani S, Afrand M, Mahmoudi B, Mahian O, Wongwises S. An updated review on application of nanofluids in heat exchangers for saving energy. Energy Convers Manag. 2019;198:111886. https://doi.org/10.1016/j.enconman.2019.111886
3. Bahiraei M, Rahmani R, Yaghoobi A, Khodabandeh E, Mashayekhi R, Amani M. Recent research contributions concerning use of nanofluids in heat exchangers: a critical review. Appl Therm Eng. 2018;133:137–59. https://doi.org/10.1016/j.applthermaleng.2018.01.041
4. Dalkilic AS, Kayacı N, Celen A, Tabatabaei M, Yıldız O, Daungthongsuk W, Wongwises S. Forced convective heat transfer of nanofluids – a review of the recent literature. Curr Nanosci. 2012;8(6):949–69. https://doi.org/10.2174/157341312803989006
5. Elmnefi M, Abdullah R. Experimental study of heat transfer enhancement using Al_2O_3/water and TiO_2/water nanofluids in a shell-and-tube heat exchanger. Heat Transf Res. 2021;52(18):15–37.

6. Elmnefi M, Al-Sammarraie M. An experimental study on heat transfer enhancement for double-pipe heat exchanger using Al_2O_3/water and TiO_2/water nanofluids. Heat Transf Res. 2022;53(12):1–23.
7. Bejan A. Entropy generation through heat and fluid flow. New York: Wiley; 1982.
8. Bejan A. Entropy generation minimization. Boca Raton: CRC Press; 1996.
9. Kotas TJ. The exergy method of thermal plant analysis. London: Butterworths; 1985.
10. Mahian O, Kianifar A, Kleinstreuer C, Al-Nimr MA, Pop I, Sahin AZ, Wongwises S. A review of entropy generation in nanofluid flow. Int J Heat Mass Transf. 2013;65:514–32. https://doi.org/10.1016/j.ijheatmasstransfer.2013.06.010
11. Barnoon P, Toghraie D, Eslami F, Mehmandoust B. Entropy generation analysis of different nanofluid flows in the space between two concentric horizontal pipes in the presence of magnetic field: single-phase and two-phase approaches. Comput Math Appl. 2019;77(3):662–92. https://doi.org/10.1016/j.camwa.2018.10.005
12. Bahiraei M, Mazaheri N. A comprehensive analysis for second law attributes of spiral heat exchanger operating with nanofluid using two-phase mixture model: exergy destruction minimization attitude. Adv Powder Technol. 2021;32(1):211–24. https://doi.org/10.1016/j.apt.2020.12.005
13. Khairul MA, Alim MA, Mahbubul IM, Saidur R, Hepbasli A, Hossain A. Heat transfer performance and exergy analyses of a corrugated plate heat exchanger using metal oxide nanofluids. Int Commun Heat Mass Transf. 2014;50:8–14. https://doi.org/10.1016/j.icheatmasstransfer.2013.11.006
14. Dagdevir T, Ozceyhan V. A comprehensive second law analysis for a heat exchanger tube equipped with the rod inserted straight and twisted tape and using water/CuO nanofluid. Int J Therm Sci. 2022;181:107765. https://doi.org/10.1016/j.ijthermalsci.2022.107765
15. Irshad K, Islam N, Zahir MH, Pasha AA, AbdelGawad AF. Thermal performance investigation of Therminol55/MWCNT+CuO nanofluid flow in a heat exchanger from an exergy and entropy approach. Case Stud Therm Eng. 2022;34:102010. https://doi.org/10.1016/j.csite.2022.102010
16. Marulasiddeshi HB, Kanti PK, Prakash SB, Sridhara SN. Investigation of entropy generation and thermo-hydraulic characteristics of Al_2O_3–CuO hybrid nanofluid flow in a pipe at different inlet fluid temperatures. Int J Therm Sci. 2023;193:108541. https://doi.org/10.1016/j.ijthermalsci.2023.108541
17. Mertaslan OM, Keklikcioglu O. Investigating heat exchanger tube performance: second law efficiency analysis of a novel combination of two heat transfer enhancement techniques. J Therm Anal Calorim. 2024;149:11155–69. https://doi.org/10.1007/s10973-023-12842-6
18. Azharuddin, Saini P. Thermodynamic analysis of shell and tube heat exchanger by using $AgNO_3$-graphene/H2O hybrid nanofluid. Heat Mass Transf. 2025;61:24. https://doi.org/10.1007/s00231-025-03542-y
19. Leong KY, Saidur R, Khairulmaini M, Michael Z, Kamyar A. Heat transfer and entropy analysis of three different types of heat exchangers operated with nanofluids. Int Commun Heat Mass Transf. 2012;39:838–43. https://doi.org/10.1016/j.icheatmasstransfer.2012.04.003
20. Pak BC, Cho YI. Hydrodynamic and heat transfer study of dispersed fluids with submicron metallic oxide particles. Exp Heat Transf. 1998;11(2):151–70. https://doi.org/10.1080/08916159808946559

21. Xuan Y, Roetzel W. Conceptions for heat transfer correlation of nanofluids. Int J Heat Mass Transf. 2000;43(19):3701–7.

22. Singh PK, Anoop KB, Sundararajan T, Das SK. Entropy generation due to flow and heat transfer in nanofluids. Int J Heat Mass Transf. 2010;53(21–22):4757–67. https://doi.org/10.1016/j.ijheatmasstransfer.2010.06.016

23. Saha G, Paul MC. Heat transfer and entropy generation of turbulent forced convection flow of nanofluids in a heated pipe. Int Commun Heat Mass Transf. 2015;61:26–36. https://doi.org/10.1016/j.icheatmasstransfer.2014.11.007

24. Moghaddami M, Mohammadzade A, Esfehani SAV. Second law analysis of nanofluid flow. Energy Convers Manag. 2011;52(2):1397–405. https://doi.org/10.1016/j.enconman.2010.10.002

25. Adogbeji VO, Lagouge T, Sharifpur M, et al. Heat transfer and thermohydraulic performance of TiO_2/MWCNT hybrid nanofluids under different regimes in pipe flow. J Therm Anal Calorim. 2026;151:14341–67. https://doi.org/10.1007/s10973-026-15822-8

26. Kanti PK, Sharma KV, Minea AA, Kesti V. Experimental and computational determination of heat transfer, entropy generation and pressure drop under turbulent flow in a tube with fly ash-Cu hybrid nanofluid. Int J Therm Sci. 2021;167:107016. https://doi.org/10.1016/j.ijthermalsci.2021.107016

27. Sundar LS, Shaik F. Heat transfer and exergy efficiency analysis of 60% water and 40% ethylene glycol mixture diamond nanofluids flow through a shell and helical coil heat exchanger. Int J Therm Sci. 2023;184:107901. https://doi.org/10.1016/j.ijthermalsci.2022.107901

28. Kadhim SA, Ibrahim OAAM, Al-Ghezi MKS, et al. Critical review of the use of TiO_2 nanofluid as a heat transfer fluid in the double-pipe heat exchanger. J Therm Anal Calorim. 2025;150:11995–2015. https://doi.org/10.1007/s10973-025-14531-y

29. Subramanian R, Kumar AS, Vinayagar K, Muthusamy C. Experimental analyses on heat transfer performance of TiO_2–water nanofluid in double-pipe counter-flow heat exchanger for various flow regimes. J Therm Anal Calorim. 2020;140(2):603–12. https://doi.org/10.1007/s10973-019-08887-1

30. Qi C, Luo T, Liu M, Fan F, Yan Y. Experimental study on the flow and heat transfer characteristics of nanofluids in double-tube heat exchangers based on thermal efficiency assessment. Energy Convers Manag. 2019;197:111877. https://doi.org/10.1016/j.enconman.2019.111877

31. Song J, Li L, Xu Z, et al. Experimental study on enhanced heat transfer using TiO_2–ethylene glycol–water nanofluid in a double-pipe heat exchanger. J Therm Anal Calorim. 2026;151:959–75. https://doi.org/10.1007/s10973-025-15187-4

32. Farajollahi B, Etemad SG, Hojjat M. Heat transfer of nanofluids in a shell and tube heat exchanger. Int J Heat Mass Transf. 2010;53:12–7. https://doi.org/10.1016/j.ijheatmasstransfer.2009.10.019

33. Shahrul IM, Mahbubul IM, Saidur R, Sabri MFM. Experimental investigation on Al_2O_3–W, SiO_2–W and ZnO–W nanofluids and their application in a shell and tube heat exchanger. Int J Heat Mass Transf. 2016;97:547–58. https://doi.org/10.1016/j.ijheatmasstransfer.2016.02.016

34. Ibrahim IU, Sharifpur M, Meyer JP. Experimental investigations of particle sizes effects on exergy and entropy characteristics of Al_2O_3–MWCNT hybrid nanofluid along the transitional flow regime. Case Stud Therm Eng. 2023;51:103575. https://doi.org/10.1016/j.csite.2023.103575

35. Elmnefi M, Al-Khazraji W. Numerical and experimental studies of thermal performance enhancement for parabolic trough solar collector using none-circulated CuO/synthetic oil nanofluid. Int J Numer Methods Heat Fluid Flow. 2023;33(9):3124–63. https://doi.org/10.1108/HFF-11-2022-0659

Supplementary Files

This is a list of supplementary files associated with this preprint. Click to download.

- 5Supplementarysecondlawresults.csv